The use of transmission electron microscopy with scanning mobility particle size spectrometry for an enhanced understanding of the physical characteristics of aerosol particles generated with a flow tube reactor

Emma C. Tackman¹, Devon N. Higgins², Devan E. Kerecman², Emily-Jean E. Ott¹, Murray V. Johnston², Miriam Arak Freedman^{1,3}

*To whom all correspondence should be addressed: maf43@psu.edu, 814-867-4267

Abstract

Aerosol particles are found throughout the atmosphere with considerable variety in morphological characteristics and chemical composition. Identifying and characterizing these particle attributes is a significant step toward improving our understanding of atmospheric chemistry. Many methods exist for measuring the size and spreading of Aitken mode particles, but there are few studies rigorously comparing the results generated between approaches in this field. Here, we compare two methods for assessing aerosol particles – scanning mobility particle size spectrometry (SMPS) and transmission electron microscopy (TEM). Aitken mode particles consisting of salt seed particles and seed particles coated with α -pinene secondary organic material were produced in a flow tube reactor. The same populations of particles were analyzed using both techniques to facilitate direct comparison. For ammonium sulfate particles impacted onto carbon and Si TEM substrates, diameters increased by +0% to +30% when compared to the suspended electrical mobility diameters, an unexpectedly wide range for a single component system. Coated particles had unpredictable diameter differences, sometimes evaluated at larger and sometimes smaller sizes after impaction when compared to the corresponding SMPS electrical mobility diameter, from -34% to +60%. While all particles were generally round in shape, variation in

¹Department of Chemistry, The Pennsylvania State University, University Park, PA 16802, USA ²Department of Chemistry and Biochemistry, University of Delaware, Newark, DE 19716, USA ³Department of Meteorology and Atmospheric Science, The Pennsylvania State University, University Park, PA 16802, USA

particle morphology was also observed in coated samples. Between 0% and 98% of particles displayed obvious phase separation suggesting more population-level diversity than expected from these particle generation processes. Characterizing the differences between TEM and SMPS results better elucidates the role of a substrate where present and shows nonequivalence in particle size distributions obtained from different instruments.

Introduction

Environmental aerosol particles are highly diverse in size and composition and are ubiquitous in the atmosphere. The physical properties of aerosol particles have important implications for atmospheric chemistry as particle size and morphology modulate a particle's chemical reactivity, light absorption and scattering properties (Radney et al. 2014; Veghte et al. 2016; Veghte and Freedman 2012), and ability to nucleate clouds (Altaf et al. 2018), as well as other chemical factors. Atmospheric particles can be internally or externally mixed and are constantly evolving, leading to enormously complex populations of ambient particulate matter (Riemer et al. 2019; Prather, Hatch, and Grassian 2008). Successful use of atmospheric models is predicated on the ability to assess characteristics of aerosol particles in order to predict the type and magnitude of their impact (Charlson et al. 1992; Riemer et al. 2019). To this end, many methods for assessing the physicochemical attributes of aerosol particles have been developed.

Several reviews including Ault and Axson (2017) outline the various spectroscopic and microscopic techniques that have been applied to the study of atmospheric aerosol particles (Ault and Axson 2017; Laskin et al. 2016; Riemer et al. 2019; McMurry 2000; Prather, Hatch, and Grassian 2008). By number, most of the aerosol particles in the atmosphere are submicron and a majority are in the Aitken mode (< 100 nm diameter) (Seinfeld and Pandis 2016). This small size

range can be prohibitive for the application of optical characterization techniques for the study of fine particles due to the Abbe diffraction limit

(1)
$$Diffraction Limit = \frac{1.22\lambda}{2NA}$$

where the smallest size accessible to an optical technique is limited by the wavelength of light (λ) and the numerical aperture (NA) (Bell and Morris 2010). Therefore, diffraction-limited techniques including brightfield optical microscopy are restricted to analysis of particles greater than 200 nm under ideal conditions, although in practice this minimum size is frequently larger. Methods for chemical characterization of aerosol particles like the aerosol mass spectrometer focus on the chemical composition and are not constrained by the diffraction limit, but they rely on other analytical tools for evaluating important physical characteristics of aerosol particles like size or shape.

Flow tube reactors are used to study a specific point in an aerosol reaction, for example secondary organic aerosol formation. Flow tube reactors are ideal for sampling and analysis over an extended period of time, since particles exiting the reactor at different times have the same physicochemical properties. Because of the chemical and physical complexity found in populations of environmental aerosol particles, laboratory-generated proxy particles are used commonly for systematic analysis of aerosols under controlled conditions. In a flow tube reactor, secondary organic material is formed from the oxidation of terpenes or other primary volatile organic compounds. Particles that contain both inorganic and organic components can phase separate and adopt a core-shell configuration where an organic shell coats the inorganic core (Miriam Arak Freedman 2017; You et al. 2012; Gorkowski, Donahue, and Sullivan 2020). Secondary organic material can be formed through condensation or reactive uptake of the lower volatility species produced during oxidation of volatile compounds onto inorganic seeds either in

the atmosphere or in a laboratory, as with a flow tube reactor. This process can generate phase-separated aerosol particles. Identifying phase-separated morphologies in atmospheric aerosol particles is essential as reactive uptake of volatile species (Zhang et al. 2018; Cohen, Quant, and Donaldson 2020), chemical properties like pH (Dallemagne, Huang, and Eddingsaas 2016), and optical properties like hygroscopicity (Zardini et al. 2008; Li et al. 2021) all differ in a phase-separated particle from a compositionally equivalent homogeneous particle. Particle generation conditions are tuned in a flow tube reactor through seed particle and reactive gas-phase species inputs and relative humidity control. The dependence of the physical properties of the resulting aerosol particles on generation conditions can be examined by further characterization methods (Krasnomowitz et al. 2019; Higgins et al. 2022).

Scanning mobility particle size (SMPS) spectrometry is a commonly used technique among many that have been developed to characterize populations of fine and ultrafine ambient particles or particles generated in a laboratory setting. A SMPS is composed of a differential mobility analyzer (DMA) and a condensation particle counter (CPC) and is used for determining the size distribution and number concentration of populations of aerosol particles with a lower particle size limit of a few nanometers and an upper size limit of several hundred nanometers. SMPS are versatile with the ability to rapidly measure electrical mobility diameter across a broad range of particle sizes. The DMA within a SMPS can be used to isolate particles of a specific size and exclude particles outside of the desired size selection for further study. In a tandem configuration, SMPS instruments can measure properties like hygroscopicity or volatility based on changes in particle diameter over time (K. Park et al. 2008). While SMPS provides valuable sizing data for particle populations, it is frequently paired with other techniques to provide information about aerosol particle morphology such as shape or phase state (K. Park et al. 2008). Shape is an

important characteristic for aerosol particle analysis that is not accounted for when all particles are assumed to be spherical, as is the case with a SMPS. Non-spherical particles (e.g., nanowires and aggregates) have mobility diameters that can deviate dramatically from volume- or surface area-equivalent diameters (K. Park et al. 2008; Lall and Friedlander 2006; DeCarlo et al. 2004). Because of these discrepancies, SMPS and further instrumentation in combination are needed to fully define mobility diameter and to convert between equivalent diameters (K. Park et al. 2008; Rogak, Flagan, and Nguyen 1993; DeCarlo et al. 2004).

Transmission electron microscopy (TEM) can measure the size, shape, and internal structure of a sample and the technique is readily applied to the study of atmospheric aerosol particles, providing a projected area-equivalent diameter or similar (Pósfai and Buseck 2010; Ott et al. 2021; Buseck et al. 2000). Using TEM, the diffraction limit associated with optical techniques can be overcome by using electrons instead of light to assay the sample allowing for the analysis of objects as small as a few nanometers in size. TEM detects electrons transmitted through a sample, so the internal structure of electron-transparent samples is accessible which is unavailable to many other tools. This benefit is especially of interest to the atmospheric aerosol sciences as individual particle morphologies can be observed directly (Li et al. 2021; Pósfai and Buseck 2010; Alstadt et al. 2018; Veghte, Bittner, and Freedman 2014; Wise et al. 2008; Fu et al. 2011; Ott and Freedman 2020; Veghte, Altaf, and Freedman 2013; Dang et al. 2022; Ching et al. 2019). For this application, TEM has advantages over other options for physical characterization of aerosol particles. Where other methods like atomic force microscopy (AFM) or scanning electron microscopy (SEM) examine the surface or near surface layer of submicron particles, brightfield TEM can distinguish between multiple phases of a single particle based on image contrast between the differing Z-number of the elements of their respective components (Veghte, Bittner, and Freedman 2014). One advantage of both TEM and AFM is individual particle analysis. Single particles within externally mixed populations can have different chemical and physical properties (Riemer et al. 2019). This diversity is lost in characterization methods that rely on population averaging, like SMPS.

Microscope analysis of aerosol particles is fundamentally different from analysis in a gas flow since the former is subject to surface or substrate effects while the latter is dependent on particle shape and density (DeCarlo et al. 2004). Generally, aerosol particles must be deposited onto a substrate for microscope investigation. Surface or substrate effects are only sometimes recognized in literature but can influence particles in important ways. It has been shown that aerosol particles with liquid or viscous components can spread or splatter upon impaction (Ott et al. 2021; Miriam A. Freedman et al. 2010; O'Brien et al. 2014; Lee et al. 2019; Olson et al. 2019; Sobanska et al. 2014; Morris et al. 2016; Bondy et al. 2017; Reid et al. 2018; Lei et al. 2022; Ray et al. 2019) and stiff particles or agglomerates may fragment (Kihong Park, Kittelson, and McMurry 2004). The degree to which a liquid particle will spread on a surface depends on adhesion and restoration forces, both contingent upon viscosity (Miriam A. Freedman et al. 2010; O'Brien et al. 2014; Lee et al. 2019; Olson et al. 2019; Reid et al. 2018; Lei et al. 2022; Ray et al. 2019; Dahneke 1971; Slade et al. 2019). Solid particles can also deform and spread during deposition (Miriam A. Freedman et al. 2010; Lee et al. 2019; Morris et al. 2016). Some aerosol particles that spread on impaction restore and leave a residue on the substrate (Miriam A. Freedman et al. 2010). Morris et al. saw that particles that undergo relative humidity cycling may experience anisotropic growth, spatially limited by this residue (2016). Veghte et al. determined that the energy of impaction is not sufficient to change the morphology of dried binary particles from homogeneous to core-shell or vice versa (2014).

Aerosol particles in the Aitken mode can have different compositions and morphologies than larger particles and are influenced more strongly by the Kelvin effect as they have small radii and high curvature (Miriam Arak Freedman 2017; Veghte, Altaf, and Freedman 2013; Seinfeld and Pandis 2016). Studies that consider submicron aerosol particle surface interactions have largely examined unsized populations of particles in the accumulation mode (100 to 1000 nm diameter) (K. Park et al. 2008; Miriam A. Freedman et al. 2010; O'Brien et al. 2014; Lee et al. 2019; Olson et al. 2019; Morris et al. 2016; Lei et al. 2022; Ray et al. 2019; Kihong Park, Kittelson, and McMurry 2004; Laskina et al. 2015). Additionally, simplified single component or binary mixtures are sometimes used to model core-shell behavior (Lee et al. 2019; Morris et al. 2016; Ray et al. 2019). Two studies included investigations of the surface interactions of complex secondary organic/inorganic particles after size selection using SMPS, but also focused on the accumulation mode (Olson et al. 2019; Lei et al. 2022). Studies of this type of interaction for particles of atmospherically-relevant complexity in the Aitken mode have not been conducted.

Here, we examine the capabilities of SMPS and TEM for analyzing atmospherically relevant Aitken mode aerosol particles. For our study, populations of salt seed particles and organic-coated salt particles generated under high and low secondary organic growth conditions are produced in a flow tube reactor. Particle populations at discrete size selections are assessed for growth by SMPS and subsequently examined using TEM. Using the same particles makes direct comparisons between the two techniques available and narrow size distributions after size selection make these comparisons more straightforward. In this work, we will show:

- For bare ammonium sulfate seeds at < 15% RH:
 - Seed particles spread after impaction. The degree to which they spread varies from +0% to +30%.

- AFM and SEM analysis shows that bare particles do not flow along the surface and have a low spreading ratio.
- For low growth samples (ammonium sulfate seeds coated in α-pinene secondary organic material generated with low precursor concentrations):
 - Particles are smaller after impaction by a percent difference of -6% to -9%.
 - TEM analysis indicates that samples of these coated particles display core-shell morphology with between 19% and 84% frequency.
 - AFM analysis demonstrates that low growth particles do not flow along a substrate,
 but have a higher spreading ratio than bare ammonium sulfate seeds.
- For high growth samples (ammonium sulfate seeds coated in α-pinene secondary organic material generated with high precursor concentrations):
 - □ Median particle diameter after impaction is sometimes larger and sometimes smaller by a percent difference of -36% to -60%.
 - TEM shows that the frequency of particles with obvious core-shell morphology in these samples is between 0% to 84%.
 - AFM analysis for high growth particles shows significant spreading along the substrate indicated by a low contact angle as well as the highest spreading ratios.

Overall, a surprisingly high level of diversity is identified for spreading for seeds and both spreading and morphology for coated particles.

Methods

SMPS and TEM experiments

For aerosol particles generated at the Pennsylvania State University, a 0.1 wt% ammonium sulfate (≥99%, Sigma-Aldrich; ACS Grade, Millipore) solution was aerosolized using a constant output atomizer (TSI 3076). The resulting particles were passed through a diffusion dryer which rapidly decreased the relative humidity to <10%. The dried particles were size selected using an electrostatic classifier (TSI 3080) and a DMA (TSI 3081) at a sheath flow to sample flow ratio of 10:1. Particles were impacted onto a substrate at the lowest stage (F) of a cascade impactor (8-stage mini-MOUDI, Model 135, MSP Corp., 2 lpm). Here, the impactor functioned primarily as a stable environment for impaction onto the substrates rather than a tool for particle size selection. For all TEM experiments, particles were impacted onto either copper-supported 200 mesh continuous carbon grids (Electron Microscopy Science) or 15 nm thick pure silicon TEM windows (Electron Microscopy Science). The continuous carbon films on the carbon/copper grids are 5-6 nm thick. All samples were stored in a desiccator and were used within 3 days of generation.

Aerosol particles prepared at the University of Delaware were generated using a flow tube reactor, as described in detail by Krasnomowitz et al., (2019) and in the supplemental information (Figure S1). Briefly, the 20.0 cm diameter, 152.4 cm long quartz tube with stainless steel funnels on each end was operated with a 6.25 L/min total flow, which produced a 4 minute residence time for particles through the reactor. The two main flows were introduced at the inlet; Flow A contained monodisperse, effloresced ammonium sulfate seed particles, ozone, and water vapor to control the RH inside the flow tube. Flow B contained the biogenic volatile organic precursor α -pinene. Particles were continuously monitored at the exit of the flow tube by an ozone monitor (Model 49i, Thermo Fisher Scientific, Inc.), RH probe (Traceable, Thermo Fisher Scientific, Inc.), and SMPS, consisting of an electrostatic classifier (TSI 3080) with DMA (TSI 3081) and a CPC (TSI 3788).

Ammonium sulfate seeds were generated by atomizing (TOPAS ATM226) a solution of ammonium sulfate (99.9995%, Sigma-Aldrich Co.) with a concentration between 100 and 400 mM. The polydisperse seeds were sent through a Nafion dryer (MD-700, Perma Pure, Lakewood, NJ) before size selection using an Electrostatic Classifier (TSI 3082 or 3080) with a DMA (TSI 3085). The monodisperse seeds were then sent into the flow tube and were continuously measured upon their exit. To sample these seeds for imaging, 1 L/min of the exiting flow was diverted through a Po charger (Model P-2021 Nuclecel Static Eliminator, NRD, LLC) and then sent into a Nanometer Aerosol Sampler (NAS, TSI 3089) for impaction onto either the copper supported carbon grids or Si window substrate.

To generate organic-coated seeds for aerosol growth samples, α -pinene (98%, Sigma-Aldrich Co.) was injected into a heated flow using a syringe pump (Model 300, New Era Systems, Inc.) and upon mixing with ozone at the inlet of the flow tube, grew the monodisperse ammonium sulfate seeds. Depending on the specific experiment being performed, the mixing ratios in the flow tube were between 10 and 100 ppbv for α -pinene and between 200 and 350 ppbv for ozone. These flows were allowed to equilibrate for an hour before sampling using the NAS onto the desired substrate.

Grids impacted with sample were packed in desiccant immediately and stored in a freezer. Special care was taken in maintaining a desiccated environment around the particles at all times to prevent the changes in particle morphology caused by freezing and subsequent thawing seen by Laskina et al. (2015). Batches of prepared samples were shipped overnight when possible from the University of Delaware to the Pennsylvania State University on dry ice to prevent moisture from accumulating during transfer. After arrival, grids were stored in a desiccator and analyzed at the Pennsylvania State University promptly, typically within 1 week of receipt.

TEM analysis of generated particles was conducted on a Tecnai LaB6 (Tecnai G20 20 XTWIN, FEI) and a Talos F200C (FEI) with cryo box functionality. Single tilt cryo-holders (Gatan) were employed for all samples, which cooled the grids to cryogenic temperatures using liquid nitrogen after insertion into the TEM for increased sample stability under the electron beam. A cryo box was used for Talos experiments for similar reasons, both to maintain low temperatures around the samples and shield them from additional moisture which could freeze onto the grid surface and cause interferences in imaging. Even at low temperatures, organic coatings rapidly damage under exposure to the electron beam so care is taken to image very quickly. An image is usually acquired within 2 seconds of exposure. Imaging was performed at a minimum of three points on each grid to avoid any local size gradient effects beneath the impaction orifices. We aim for 100 to 200 particles per sample, although many fewer measurements than this are needed to fully define the shape of a very narrow histogram. ImageJ software (NIH) was used to analyze TEM images for morphology and area-equivalent diameters for each particle. Within ImageJ, particles were manually identified and measured to prevent biases that might be introduced by batch processing. Aggregates and overlapping particles were rare due to low particle concentrations but were removed from analysis when identified. TEM data is binned for visualization only.

AFM experiments

AFM samples of seeds and coated particles were generated in the same manner as the TEM samples at the University of Delaware with a cleaned Si wafer chip (Virginia Semiconductor) as the substrate instead of a carbon grid or Si window. A small number of seed samples were also generated at the Pennsylvania State University to ensure that the Si wafer substrate and the cascade impactor were compatible and that the two substrates provided equivalent spreading results. Si

wafers were again stored in desiccant and transferred overnight from the University of Delaware to the Pennsylvania State University. AFM experiments were conducted at the Pennsylvania State University on a Dimension Icon AFM in tapping mode (Bruker). A dry N₂ gas purge was used to maintain a low relative humidity, typically below 20%, within the AFM enclosure. Dry conditions were necessary to prevent the deliquescence of salt samples during analysis.

Results and Discussion

Seed particles

Ammonium sulfate is a well-characterized aerosol component commonly chosen as a laboratory model due to its prevalence in continental aerosol. Seed particles made of ammonium sulfate were used to compare the median size of particles measured with SMPS to the median size of those same particles as measured with TEM. For size-selected samples, ammonium sulfate particles were selected at specific mobility diameters with an electrostatic classifier and DMA and measured via SMPS, after which the same population of particles was collected onto TEM grids or equivalent substrates. Figure 1 shows a typical size distribution for a population of SMPS size-selected particles after generation but before impaction (solid curve) and the same particles measured by TEM after impaction onto a substrate (vertical bars). Both measurement techniques give a narrow size distribution for this single component system after size selection, as expected, where the width and shape of the SMPS distribution are defined by the transfer function (Stolzenburg and McMurry 2008; Veghte and Freedman 2012). The size distributions in Figure 1a show both singly- and doubly-charged particles transmitted by the DMA. Refer to the Supplemental Information for more details on particle size distributions.

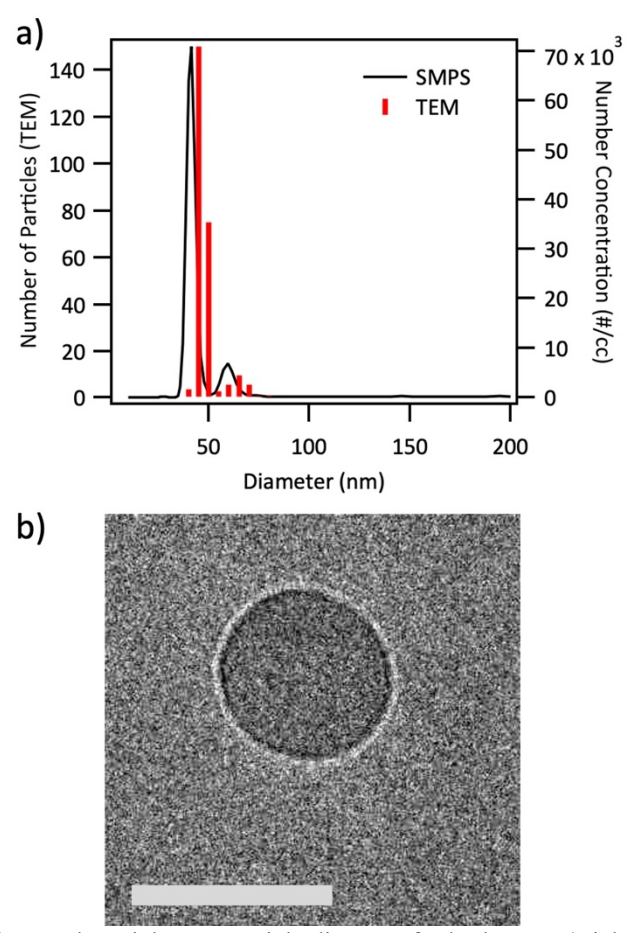


Figure 1. a) The number of aerosol particles vs. particle diameter for both TEM (sticks) and SMPS (solid line) for a representative sample of bare ammonium sulfate particles size selected at 40 nm. The diameter of the particles given by SMPS is the mobility diameter (D_m) while the diameter given by TEM is the projected area diameter (D_{pa}) after impaction. The positive offset of the D_{pa} distribution from D_m indicates the influence of the substrate surface on the particle. **b)** A representative TEM image of a bare ammonium sulfate seed particle. Scale bar 50 nm.

Here, as in all cases for bare ammonium sulfate, particles had a larger median diameter after impaction as indicated by the TEM-derived distribution being positively offset from the distribution given by SMPS. This increase in diameter is attributed to interaction between the particle and the substrate surface, specifically spreading. Within a SMPS, aerosol particles in a gas flow pass by a radiation source. The particles then enter a DMA where most particles are neutralized, but some pick up a charge and are then sorted according to their electrostatic mobility and counted with a CPC. Thus, the diameter measured by SMPS is the mobility diameter (D_m) of a suspended particle, which is equal to the volume equivalent diameter for spherical particles.

While it is not necessary to consider substrate interactions for suspended particle populations, these interactions cannot be disregarded after the sample is deposited onto a surface. TEM shows a collapsed two-dimensional representation of the three-dimensional structure projected onto the X-Y substrate plane, yielding a projected area-equivalent diameter (D_{pa}) for a particle on a substrate. Table 1 summarizes the median SMPS mobility diameters and projected area diameters measured by TEM as well as the percent difference for each sample calculated by Equation 2:

(2)
$$Percent \ Difference = \left(\frac{D_{pa} - D_{m}}{D_{m}}\right) \times 100$$

where the percent difference is a measure of how the median D_{pa} differs from the median D_{m} , in both sign and magnitude. Explicitly, a positive percent difference indicates that D_{pa} is greater than D_{m} and that the median particle diameter increased after impaction. Nominal particle mobility diameters of 40 nm, 60 nm, 80 nm, and 100 nm were chosen for this study, and replicate trials were run at each size. Results for samples generated at the Pennsylvania State University report nominal median mobility diameters only as the precise median values were not measured via SMPS. All other samples report precise median values for the mobility diameters of each population of particles. The D_{pa} for the impacted ammonium sulfate particles at all sizes were found to be larger than their suspended counterparts, spreading by a percent difference from +0% to +30% after impaction. This range in percent difference represents a range of diameter changes between +0.1 nm and +18.8 nm, or the maximum and minimum values derived from calculating the difference between the Median (TEM) column and the Median (SMPS) column for each line in Table 1. Further details on TEM imaging of salt particles can be found in the Supplemental Information.

Table 1. SMPS and TEM analysis of ammonium sulfate seed particles

Substrate	Generation	n ^a	Median (SMPS) ^b		% difference ^d	
		53	39.9 nm	44.4 nm	+11%	

		111	39.5 nm	40.1 nm	+1%
		55	39.5 nm	40.1 nm	+1%
		185	40.1 nm	42.1 nm	+5%
		208	37.5 nm	48.9 nm	+30%
		127	41.6 nm	44.7 nm	+7%
	University of	129	41.5 nm	44.3 nm	+7%
	Delaware	10	61.3 nm	64.9 nm	+6%
Carbon grid		122	61.0 nm	65.4 nm	+7%
grid		185	61.1 nm	61.0 nm	0%
		111	64.0 nm	68.6 nm	+7%
		136	63.0 nm	77.3 nm	+23%
		120	62.7 nm	68.3 nm	+9%
	The	30	80 nm	85.6 nm	+7%
	Pennsylvania State	16	80 nm 87.7 nm		+10%
	University	105	100 nm	118.8 nm	+19%
		164	42.8 nm	49.1 nm	+15%
	University of Delaware	232	42.8 nm	49.0 nm	+15%
	Delaware	154	59.9 nm	72.0nm	+20%
Si window	The	117	80 nm	95.1 nm	+19%
	Pennsylvania	85	80 nm	93.9 nm	+17%
	State	121	100 nm 102.0 nm		+2%
	University	45	100 nm	100.6 nm	+1%
а					

a number of particles analyzed per sample

Notably, spreading represented by increases in particle diameter after impaction were similar for samples generated using the two different methods of impaction (i.e., cascade impactor and NAS). Here, dry ammonium salt particles are assumed to have an adequately high viscosity, or stiffness, so that they are able to recover after deformation during the impaction process to the same degree, regardless of impaction velocity (Morris et al. 2016; O'Brien et al. 2014). The range of percent differences between SMPS- and TEM-measured ammonium sulfate particle diameters was wider than expected for size selected particles of only one component, but consistent between the two experimental schemes both in sign and magnitude. The NAS at the University of Delaware used a biased substrate where oppositely-charged particles are impacted through electrostatic

b median particle mobility diameter

^c median particle projected area diameter

percent difference between the median mobility diameter and median projected area diameter as defined by Equation 2

precipitation, giving the total range of percent differences between +0% and +30%. The cascade impactor used at the Pennsylvania State University sorted particles by inertia, where the particles in a gas stream are forced to take a series of sharp turns; particles above the cutoff size of each stage are deposited onto a substrate while those below are small enough to carry on through the turn. This process provided a range of percent differences from +7% to +19% (Table 1), falling within the spreading range derived from NAS impacted samples. While electrostatic precipitation is a softer impaction method than cascade impaction, these data indicate that the two methods are interchangeable in this situation.

To gain more information about particle size and the particle-surface interface, equivalent ammonium sulfate samples were studied using AFM. AFM is a useful corollary scanning probe technique able to obtain height and surface topographical information for impacted particles that is inaccessible from a TEM. AFM samples of single component ammonium sulfate particles on Si wafer chips were made and analyzed for morphology and spreading ratios at the Pennsylvania State University. Results for experiments evaluating the equivalence of carbon and Si for TEM analysis are shown in Table 1 and discussed in the SI. Figure 2 shows a representative AFM scan for these particles as well as a line scan through the peak of a single particle, showing the particle height in profile. Line scans for these samples suggest that the bare ammonium sulfate particles met with the substrate at or near a 90° angle (Figure 2b). Due to the nature of the technique, an AFM probe is unable to consider any potential space beneath a particle with a contact angle greater than 90°. AFM imaging does confirm here that single component ammonium sulfate particles do not "flow" along a substrate surface which would be observed as a lower contact angle or outward sloping cross section. Lack of flow is supported by SEM imaging. Bare ammonium sulfate particles were further analyzed by SEM for an improved understanding of the particle-substrate

interface, although these results were primarily qualitative. For SEM studies, particles are imaged from the side in the plane perpendicular to the substrate surface using a high tilt stage. In this way, it was observed that the ammonium sulfate particles meet the substrate surface at an obtuse contact angle greater than 90° such that they sit above the substrate, forming a quasi-ellipsoid and confirming the presence of a void underneath (Figure S2).

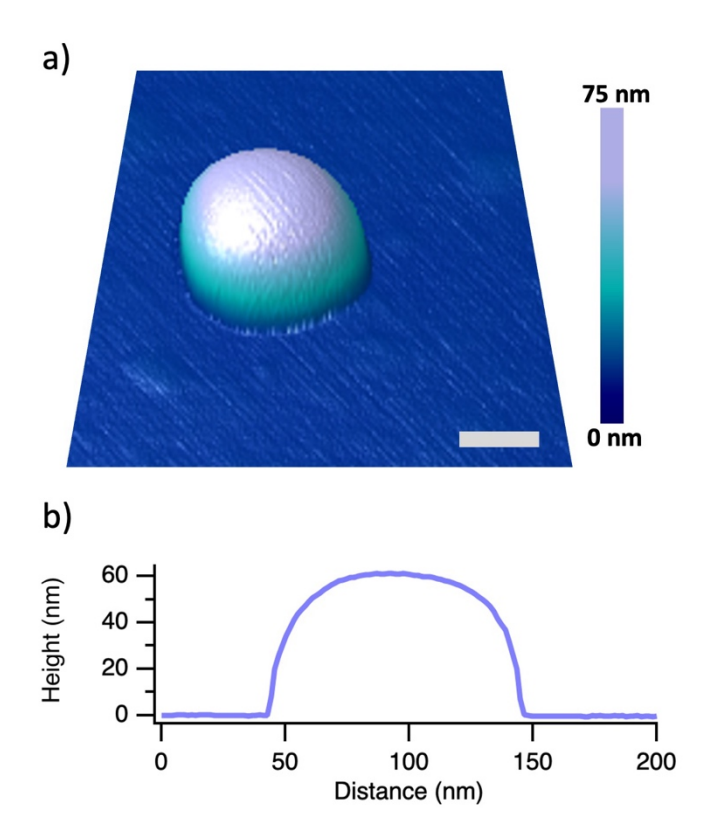


Figure 2. a) AFM height results represented in 3D for a single ammonium sulfate particle. Ammonium sulfate particles were found to be rounded in shape and homogeneous. Scale bar 50 nm. **b)** A line scan taken through the center of the particle shows that the particle meets the surface at or near a right angle. While this does not represent the void space present beneath the particle, a contact angle of 90° or below indicates the absence of particle flow along the substrate after impaction.

AFM characterization can provide a spreading ratio for individual particles, defined as

$$Spreading Ratio = \frac{D_{pa}}{h}$$

or the ratio of the projected-area diameter (D_{pa}) to particle height (h) (Olson et al. 2019; Bondy et al. 2017). Spreading ratios are a convenient dimensionless metric for assessing to what degree

particles spread along a surface after impaction as a proxy for viscosity (Bondy et al. 2017). Figure 3 presents ammonium sulfate particle spreading ratios plotted against particle diameter. Numerical results for spreading ratio calculations are summarized here and tabulated in full in Table S2. A population of bare ammonium sulfate particles had an average spreading ratio of 1.76 ± 0.29 (Figure 3). For reference, the theoretical spreading ratio for a nonwetting sphere resting on a surface would be 1 and that of a perfect hemisphere with full substrate contact would be 2. Ammonium sulfate particles are expected to be nearly spherical when suspended. While the presence of void space beneath the impacted particle indicates that there is no "flow" along the surface, an average spreading ratio of 1.76 for bare ammonium sulfate implies a higher aspect ratio than a sphere and a horizontal deformation of the ammonium sulfate particles after impaction. A spherical particle that is transformed into a perfect volume-conserved hemisphere after impaction would see an increase in diameter of +26%. Again, due to void space under the particle, in practice the impacted shape is closer to a truncated ellipsoid and so the conserved-volume diameter transformation should be somewhat less in magnitude. Even so, a theoretical value of, or somewhat less than, +26% spreading fits into the range of percent differences for ammonium sulfate particles observed in Table 1, confirming some level of spreading for impacted particles. Take note that, although they are also an evaluation of particle spreading, spreading ratios are fundamentally distinct from the percent difference calculations in Table 1.

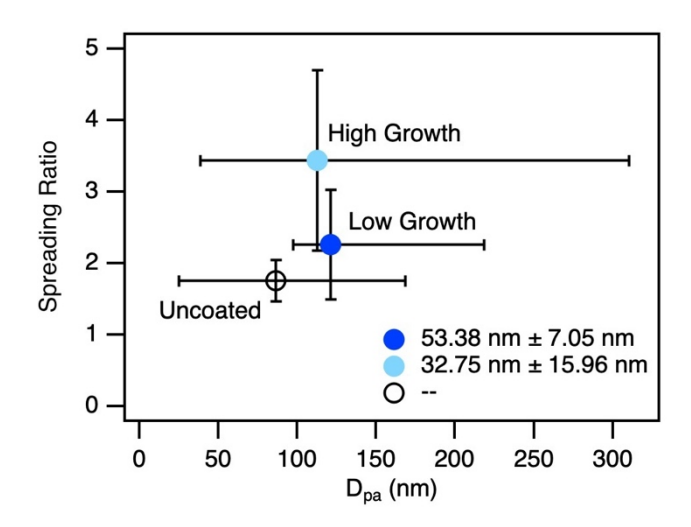


Figure 3. Spreading ratios for uncoated ammonium sulfate seed particles, seed particles with low growth in diameter due to a secondary organic coating, and seed particles with a high growth of the same vs. particle diameter. The horizontal error bars represent one standard deviation in observed particle diameters and the vertical error bars show one standard deviation in spreading ratios for each type of particle. Particle spreading ratio (y axis) and degree of coating are shown to be positively correlated while particle height (legend) and degree of coating are inversely proportional for the two coated samples.

Low growth and high growth SOA on ammonium sulfate

A coating of α -pinene secondary organic material was generated and grown onto size selected ammonium sulfate particles in the flow tube reactor at the University of Delaware, resulting in particles with a core-shell morphology. Ammonium sulfate particles acted as seeds on which a shell, or phase, of semivolatile organic material was able to grow. Here, experiments were designed to yield either "high growth" or "low growth" samples. High growth sample experiments used higher α -pinene (10-100 ppbv) and ozone concentrations (275-350 ppbv), depending on the seed particle number concentration, to yield a D_m increase of at least 11 nm. Low growth sample experiments were designed to yield a D_m increase less than 11 nm and used α -pinene and ozone concentrations of 5-10 ppbv and ~350 ppbv, respectively. Growth in all cases is defined by the total increase in diameter; an even coating of secondary organic material about a suspended particle core would have an annular shell width of half of the growth value. Growth measured by SMPS

as represented by increases to D_m should not be confused with growth determined by TEM observation. Both types of growth will be discussed and contrasted below.

Figures 4a and 5a show typical size distributions for a population of particles composed of an ammonium sulfate core surrounded by a low growth and high growth organic shell, respectively. For samples of coated particles generated for TEM analysis, ammonium sulfate seed particles were size selected before coating. Upon growth, the distribution broadens as a result of slight differences in particle residence times, resulting in slight differences in coating thickness. Another outcome of the coating process is the formation of new particles, which is observed as an additional mode in the size distribution tertiary to those of the singly-and doubly-charged particles. New particles are smaller than the seeded particles and constitute the leftmost (i.e., smallest diameter) mode in the size distribution (Figure S9). Unlike the doubly-charged particles, these are isolated and removed from D_m and percent difference calculations as well as the SMPS size distributions in Figures 4a and 5a.

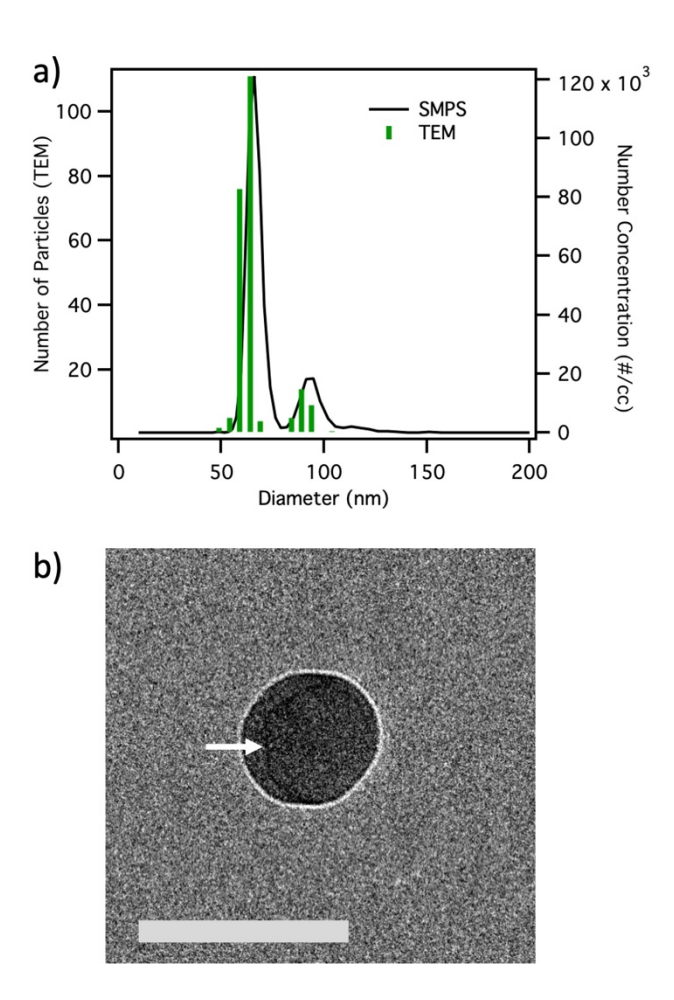


Figure 4. a) The number of aerosol particles vs. particle diameter for both TEM (sticks) and SMPS (solid line) for a representative sample of ammonium sulfate particles size selected at 60 nm with a low growth of secondary organic material. A distinct peak at $D_m < 50$ nm due to new particle formation is not shown. The distribution of projected area particle diameters given by TEM measurements was found to be slightly negatively offset from the SMPS mobility distribution **b)** A representative TEM image of an ammonium sulfate particle coated with a low growth of secondary organic material. The coating is visible as the outer portion of the particle delineated from the inner phase by a dark line (arrow). Scale bar 100 nm.

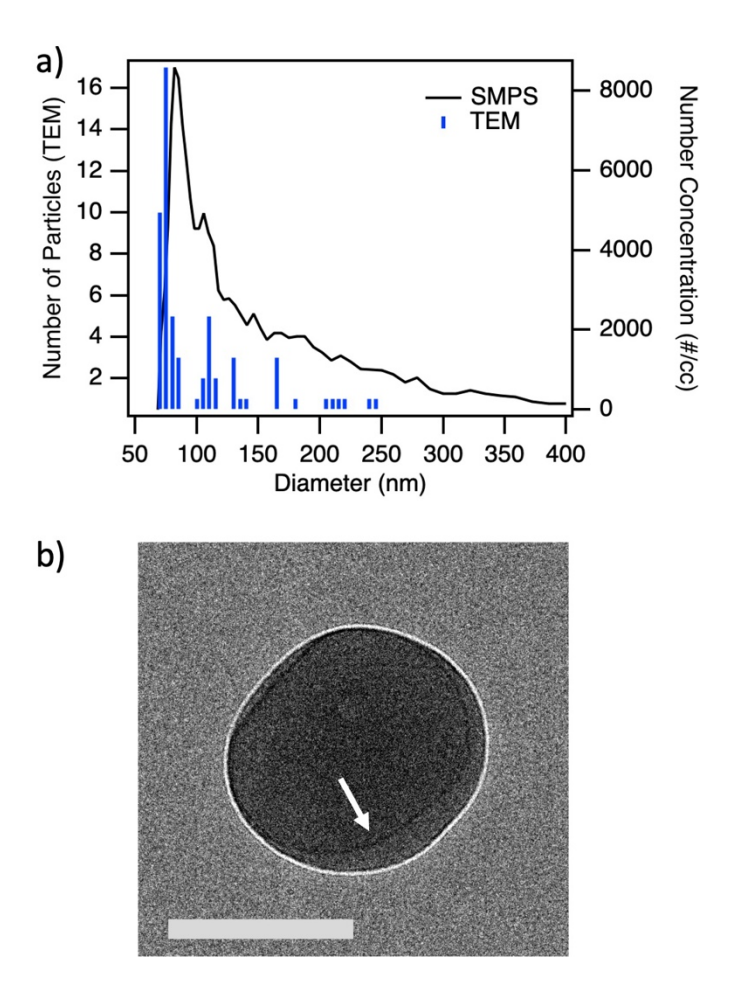


Figure 5. a) The number of aerosol particles vs. particle diameter for both TEM (sticks) and SMPS (solid line) for a representative sample of ammonium sulfate particles size selected at 60 nm and coated with a high growth of secondary organic material. A distinct peak at $D_m < 50$ nm due to new particle formation is not shown. The TEM size distribution has a significant negative offset from the SMPS mobility distribution, which itself represents a more polydisperse population due to different residence times of individual particles in the flow tube reactor. **b)** A representative TEM image of an ammonium sulfate particle with a high growth of secondary organic material. The coating is visible as the outer portion of the particle delineated from the inner phase by a dark line (arrow). Scale bar 100 nm.

Variable percent difference values between D_m and D_{pa} were observed for coated samples depending on the thickness of the coating. Surprisingly, low growth samples had consistently smaller median diameters when measured by TEM compared to the SMPS, with negative deviations ranging from -6% to -9% (Table 2). This range in percent difference represents a range of diameter changes between -2.9 nm and -5.9 nm, or the maximum and minimum values derived from calculating the difference between the Median (TEM) column and the Median (SMPS)

column for each line in Table 2. For particles with a thin layer of secondary organic material, a decrease in measured median diameter indicated the particles were smaller after impaction. A small negative percent difference in median diameters can be observed in Figure 4a by a slight negative offset of the TEM particle size distribution from the SMPS-derived one. In contrast, high growth samples showed a considerable range of median percent difference values, from -36% to +48% (Table 3). This range in percent difference represents a range of diameter changes between -31.3 nm and +33.0 nm, or the maximum and minimum values derived from calculating the difference between the Median (TEM) column and the Median (SMPS) column for each line in Table 3. While particles with high amounts of secondary organic growth showed varying magnitudes of size deviations from negative to positive divergence with no discernable trend, all of the largest percent differences in diameter, or those over +30% or under -9%, were in the high growth category. Size distributions for a high growth sample with a large negative difference are shown in Figure 5a where the TEM size distribution is at a significant negative offset compared with the SMPS results. Particle spreading for all levels of growth, quantified by percent difference values, could not be correlated to any identifiable experimental parameter including seed number concentration, α -pinene or ozone mixing ratio, relative humidity at the time of impaction, or time passed between generation and analysis. The cause of the remarkable level of diversity seen in high growth samples is not clear.

Table 2. SMPS and TEM analysis of ammonium sulfate/SOA low growth particles

Substrate	Generation	n ^a	Median (SMPS) ^b	Median (TEM) ^c	% difference ^d	%PS ^e	Growth (SMPS) ^f	Growth (TEM) ^g	Seed Size (SMPS) ^h	Core Size (TEM)
	University of Delaware	48	45.6 nm	42.6 nm	−7%	19%	5.7 nm	10.0 nm	39.4 nm	37.4 nm
		98	45.6 nm	42.4 nm	-7%	51%	5.7 nm	8.0 nm	39.4 nm	33.7 nm
		127	47.1 nm	44.2 nm	-6%	47%	4.0 nm	3.3 nm	43.1 nm	40.9 nm
		227	66.6 nm	61.1 nm	-8%	68%	5.5 nm	13.7 nm	61.1 nm	48.1 nm
		68	68.0 nm	62.0 nm	-9%	43%	5.2 nm	18.3 nm	62.8 nm	41.6 nm
		127	68.5 nm	63.0 nm	-8%	84%	5.8 nm	14.5 nm	62.8 nm	49.7 nm

Table 3. SMPS and TEM analysis of ammonium sulfate/SOA high growth particles

		a	Median	Median	d was d		Growth	Growth	Seed Size	Core Size
Substrate	Generation	n	(SMPS) ^b	(TEM) ^c	% difference	%PS ^e	(SMPS) ^f	(TEM) ^g	(SMPS) ^h	(TEM) ⁱ
		30	56.1 nm	41.7 nm	-26%	73%	16.6 nm	8.4 nm	40.0 nm	33.6 nm
		114	71.2 nm	105.4 nm	+48%	41%	30.3 nm	70.2 nm	40.9 nm	39.3 nm
	University of Delaware	92	48.0 nm	42.5 nm	-11%	7%	13.1 nm	5.7 nm	37.6 nm	32.0 nm
		121	64.4 nm	41.4 nm	-36%	92%	22.2 nm	4.8 nm	42.2 nm	36.5 nm
Carbon grid		155	62.9 nm	42.3 nm	-33%	88%	20.7 nm	4.3 nm	42.2 nm	38.2 nm
		60	101.3 nm	77.1 nm	-24%	43%	40.6 nm	5.5 nm	62.7 nm	105.4 nm
		147	103.2 nm	72.0 nm	-30%	65%	40.6 nm	5.0 nm	62.7 nm	93.8 nm
		92	77.5 nm	62.8 nm	-19%	45%	15.2 nm	25.3 nm	62.4 nm	37.0 nm
		174	77.9 nm	62.4 nm	-20%	80%	15.5 nm	24.2 nm	62.4 nm	38.4 nm
Si window		198	55 nm	82.6 nm	+50%	91%	13.5 nm	19.9 nm	41.5 nm	65.7 nm
		223	55 nm	88.0 nm	+60%	98%	13.5 nm	23.2 nm	41.5 nm	62.7 nm
		110	81.2 nm	82.5 nm	+2%	0%	19.1 nm	NA	62.2 nm	NA
		164	81.5 nm	69.1 nm	-15%	18%	19.3 nm	5.3 nm	62.2 nm	78.9 nm

Column descriptions found in notes below Table 2

Beyond size analysis, particle morphology was investigated as well, specifically evaluating for the presence of multiple phases. The core-shell morphology of organic-coated ammonium sulfate particles is readily apparent using TEM because of the contrast in electron densities between the two phases (Figs 4b and 5b). Unexpectedly, not all coated particles displayed obvious core-shell phase character when imaged. Our experiments indicated a large range in the proportion of phase separated particles, from 0% to 98% of the total number of particles presenting a clear secondary organic phase in addition to the ammonium sulfate core (Tables 2 and 3). One possible

a number of particles analyzed per sample

median particle mobility diameter

^c median particle projected area diameter

^d percent difference between the median mobility diameter and median projected area diameter as defined by Equation 2

e percent of particles displaying obvious phase separation

^f particle growth observed by SPMS defined by the difference in D_m before and after the coating process

 $^{^{}g}$ particle growth observed by TEM defined by the difference between the D_{pa} of the full particle and the D_{pa} of the core phase, or else twice the shell thickness

median D_m of the seed particles before coating

median D_{pa} of the core phase in the coated particle

explanation for this large range is that the secondary organic coating is composed of many different chemical species, some of which might be similar in density to the ammonium sulfate core with respect to the TEM electron beam. If these species are predominant, then there will be little difference in the electron transparency between the two phases and they might appear as a single continuous phase. Evidence of varying chemical composition in the secondary organic coating of individual core-shell particles within a similar population has been presented from mass spectrometry and nano-aerosol mass spectrometry studies (Kerecman et al. 2021; Tu and Johnston 2017). Additionally, phase separation did not show any size dependence, as both homogeneous and core-shell particles were observed at large and small sizes within populations of coated particles.

Particles displaying core-shell morphology were further analyzed for coating thickness and core diameter. The growth values for TEM measurements displayed in Tables 2 and 3 are based on the observed shell thickness calculated as the difference between the total D_{pa} for each coated particle and the D_{pa} of the core. As discussed previously, growth values for SMPS consider the difference in D_{m} of the suspended particles before and after coating with secondary organic material. There is again no obvious trend in the difference between growth evaluated by SMPS and TEM. For low growth core-shell particles, the median shell thickness observed with TEM was greater than the increase in particle diameter with secondary organic growth measured by SMPS for all but one sample (Table 2). The high growth samples showed shell thicknesses both greater than and less than the amount of growth measured by SMPS for both the 40 nm and 60 nm seed particles (Table 3) Further, the core diameters for core-shell particles in growth samples were measured by TEM and compared to the D_{m} values for the seed particles measured by SMPS after size selection and before coating with secondary organic material. The diameter of the suspended

seeds before coating was always larger than the observed diameter of the core phase after impaction for low growth samples. For high growth samples, the difference between these values were variable and also showed no trend between SMPS and TEM measurement techniques.

Additionally, heterogeneity in morphology between populations could be a result of particle generation in a flow tube reactor. As previously described, different pathways for individual particles through a flow tube reactor would lead to broadening of the size distribution for growth samples. The extent of this broadening effect is dependent on the concentration of the seeds and the precursors for the secondary organic material. Minor differences in these concentrations can have outsized effects on the amount of organic material on particles, causing further differences between populations of particles generated under ostensibly identical conditions. It is likely that these population-level variations are reflected in the large range of percent differences for high growth populations, and to a lesser extent, in the variety of percent differences observed for low growth populations (Tables 2 and 3).

In all, no apparent trends were observed for the morphological analysis of core-shell aerosol particles between SMPS and TEM, either for percent phase separation or in the thickness of the shell phase or the diameter of the cores. Determination of morphology may depend in part on coating thickness where secondary organic material abundance is insufficient to form a complete shell. In these cases, particles with a patchy organic coating or partially engulfed structure would be classified as core-shell phase separated for the purposes of this study if the coating is visible and obvious. In less obvious cases, a very patchy secondary organic layer could be too difficult to distinguish from the core depending on the orientation of the particle relative to the electron beam. Both the angle of particle impaction and the incident angle of the electron beam during microscope analysis depend on the flatness of the substrate (Figures S3 and S4). In samples

with very thin coatings, an underrepresentation of coated particles could lead to variety in the number of phase-separated particles counted, and therefore, TEM-measured median shell thicknesses.

In the same manner as the uncoated ammonium sulfate seeds, the coated particles were examined using an AFM to assess height and spreading ratios. Again, supplementary TEM experiments on Si windows were conducted. These results are shown in Table 3 and discussed in the SI. The low and high growth secondary organic coatings were visually distinct when observed by AFM; the low growth particles were primarily round and uniform in shape contrasting with the high growth sample which were much more heterogeneous and irregular. Such irregularity in high growth samples may have been the result of coagulation of seed particles and new particles. Like uncoated seed particles, low growth particles were topographically smooth and rounded (Figure 6). Line scans showed a contact angle at or below 90° signifying little to no flow of the organic shell along the substrate surface, as was observed for the seed particles (Figure 6b). These results are consistent with our SEM observations of salts and salt/organic binary systems. SEM images of ammonium sulfate particles coated in a model organic phase of 2-methylglutaric acid demonstrate interactions between the coating and the substrate comparable to the bare ammonium sulfate sample. The particles appear ellipsoidal with a large contact angle and no outward flowing character (Figure S2). In contrast, AFM imaging for high growth particles shows a small contact angle that can be seen in a line scan along with particle sides sloping up to a plateau demonstrating high wettability of the coating, or significant flow along the substrate (Figure 7). In addition, there are indications of internal structure (i.e., core-shell morphology) within the high growth particles in the AFM images. Variations in the probe adhesion and indentation channels point toward chemical differences across regions of some particles indicating the two distinct phases (Figure

S11). Some particles with high secondary organic growth show step-like differences in height which suggest different viscosities or affinities for spreading along the substrate surface between phases within a single particle (Figure 7b). Pronounced phase character in high growth particles supports TEM observations of core-shell particles in growth samples.

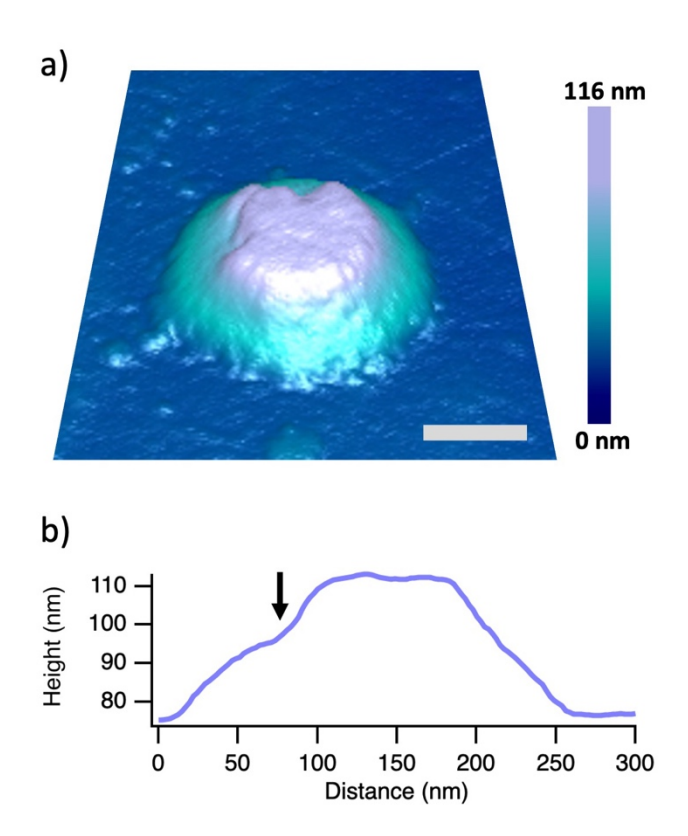


Figure 6. a) AFM height results represented in 3D for a single ammonium sulfate particle with a low growth coating of secondary organic material. Low growth particles were found to have similar topographical features to bare particles with a smooth rounded surface. Scale bar 50 nm. **b)** A line scan through the center of the low growth organic-coated particle looks similar to that of the bare seed particle as well. The contact angle of the particle indicates no flow of the organic coating along the substrate.

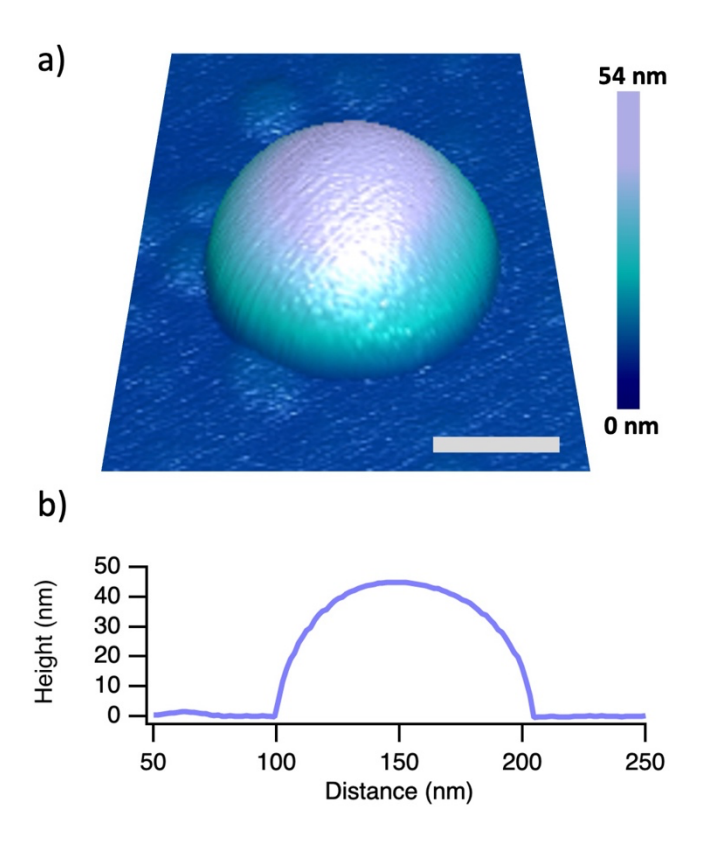


Figure 7. a) AFM height results represented in 3D for a single ammonium sulfate particle with a high growth coating of secondary organic material. These particles were found to have irregular surfaces with internal features possibly indicating core-shell morphology. Scale bar 100 nm. **b)** A line scan taken through the center of the particle shows that the particle meets the surface at a contact angle less than 90°. The line scan also shows a step-like feature demonstrating a possible internal phase boundary (arrow).

Spreading ratios for the various regimes of secondary organic growth represent the different degrees to which model aerosol particles spread on substrates with more spreading corresponding to a larger spreading ratio. AFM observations of coated particles confirm the hypothesis that higher amounts of growth, or thicker organic coatings, spread more along a substrate surface than bare particles with no coating. A positive correlation was observed between the degree of organic coating and average spreading ratio (Figure 3, y axis). Particles with a high growth of secondary organic material had the highest spreading ratios and bare particles had the lowest with low growth particles exhibiting intermediate spreading ratio values. High spreading ratios explain some of the size disparities observed for coated particles between SMPS and TEM

as the spreading of the organic coating in high growth samples likely accounts for some portion of the largest positive percent differences between D_m and D_{pa} .

It is clear that spreading alone cannot explain all of the discrepancies between SMPS and TEM measurements, and transformations of particle volume should be considered as well. One important point to reiterate is that trends in spreading ratio do not correlate to trends in diameter percent differences. While both are measures of particle-surface interactions, a percent difference compares suspended to impacted diameters and a spreading ratio considers interactions between the particle and the substrate specifically. Low growth samples illustrate this point. As Table 2 shows, median D_{pa} is smaller than median D_{m} for size-selected low growth particles meaning particles have smaller diameters when observed on a substrate leading to negative percent differences, contrasting with the intermediate low growth spreading ratios established in Figure 3. It is possible for a coated particle to both spread after impaction with a higher spreading ratio than a bare seed particle and have a smaller D_{pa} than D_{m} , as is the case with low growth particles. For these two conditions to be met simultaneously, though, an additional physical or chemical factor must also be resolved as these conditions indicate that the total particle has lost volume.

Various physical or chemical transformations might reduce total particle volume in low growth particles. One such chemical consideration is the loss of volume caused by particle phase chemical reactions occurring at the interface between the organic shell and the ammonium sulfate core. Diminished particle volume could result from the consumption of the core phase to form organosulfates paired with an ensuing increase in overall particle density. Lei et al. (2022) and Olson et al. (2019) report the formation of organosulfates in SOA-coated sulfate particles. Physical changes to the ammonium sulfate core may also influence particle volume. Beaver et al. saw an increase in ammonium sulfate density after dissolving the salt and then drying the solution back to

a solid (2008). This increase in density may indicate the presence of voids creating spaces within the initial ammonium sulfate crystals, supported by the microrestructuring of ammonium sulfate particles described by Mikhailov et al. (2009). If present in the ammonium sulfate cores of the particles studied here, these voids could collapse upon impaction of the particle leading to an increase in density and loss of volume. For a particle that spreads along a substrate but also experiences collapses in voids after impaction, a negative percent difference would be observed while maintaining an elevated spreading ratio so long as the decrease in D_{pa} due to volume loss exceeds the increase due to spreading. This scenario is expected to be most relevant for low growth samples with thin coatings.

Both chemical and physical considerations of volume loss also pertain to high growth samples, although samples with very thick secondary organic coatings may see a sufficient increase in D_{pa} due to spreading of the organic phase such that D_{pa} is still greater than D_m and a positive percent difference is observed. We suggest this is the case for high growth samples with positive percent differences in diameter (Table 3). For both low and high growth samples, volume loss may also result from the loss of volatile organic compounds under the vacuum conditions experienced during TEM analysis. High growth samples with large negative percent differences could in part be the result of a reduction in particle volume due to the depletion of semivolatile species. Park et al. saw a 3 nm decrease in particle diameter from semivolatile loss under vacuum conditions (2004). While Park et al. studied diesel exhaust particles, we expect the secondary organic material present our work to be more volatile than diesel exhaust. Loss of volatile organic compounds is more likely for larger particles due to the Kelvin effect as high vapor pressure over small particles (> 50 nm diameter) means that only low volatility species will condense to form a coating on small seeds. Larger particles are able to take up semivolatile compounds as well which

are more easily lost in high vacuum conditions. For all samples of coated particles, it is likely that sufficient chemical or physical volume loss accounts for the negative deviations observed between D_m and D_{pa} in some growth samples while the viscous organic shell phase gives rise to high spreading ratios.

To ensure the shipping process and storage conditions did not significantly influence the properties of the aerosol particles, two parallel control experiments were performed and are described in the SI. These experiments suggest that, if stored under the dried conditions of this study, both semivolatile single component and secondary organic coatings are stable for periods far exceeding the time between generation and analysis for particles in this study. An interesting result of these trials shows that for both sets of control samples there is a slight trend in increasing core size and slight decrease in shell thickness over time (Tables S3a and S3b). These together could signal interesting chemical processes occurring at the phase boundary. One possibility is that reactions at the interface consume ammonium sulfate in the core to form organosulfates, as mentioned previously. Because this trend is observed over the course of several weeks, it is likely that the particle volume loss seen over shorter spans of time needed to generate and analyze the low and high growth particles are attributed to one of the other suggested volume loss mechanisms and that organosulfate formation is negligible during the storage times for typical particle analysis. Although these small trends may be within error for the measurement, ongoing particle phase reactions have implications for morphology or additional reactivity between phases and reactive uptake of gas phase species and should be investigated further.

Implications and Conclusions

SMPS and TEM were used together to determine the influence of a substrate on the size of Aitken mode aerosol particles serving as atmospheric proxy systems. SMPS and TEM are complementary high throughput techniques often used for assessing the physical properties of aerosol particles. The use of TEM in this study also allowed for the morphological assessment of coated particles. Our results indicate that an unexpectedly wide variety in spreading values can be observed for samples of aerosol particles after deposition onto a surface, even with environmental model systems containing one component. Uncoated salt particles had positive percent differences and the lowest spreading ratios. Even wider variation in spreading is seen for particles composed of salts and a coating of secondary organic material. Low growth particles had thin coatings of secondary organic material on an ammonium sulfate seed particle and were characterized by slightly higher spreading ratios than bare ammonium sulfate particles and percent differences in diameter of negative sign and small magnitude. This result suggests particle density changes either physically upon impact or chemically over time. High growth particles had thick secondary organic coatings and were distinguishable by large percent differences in diameter and the highest spreading ratios of the three coating regimes.

Because our results show particle size changes after impaction for virtually all samples, caution is recommended when reporting exact sizes for particles that have been deposited onto a substrate, as with techniques like AFM, TEM, or SEM. However, although particles are transformed by impaction or the presence of a substrate, analyzing broad trends in size is likely to be acceptable. Additionally, those using SMPS to assess particle populations should be wary of morphological variation between sample populations that can appear to be identical to a SMPS, as seen in our data for particles generated in a flow tube reactor. The work presented here shows that TEM can reveal some of this variation, and this phenomenon deserves further consideration in

future studies. These findings also influence how TEM data can be interpreted. When calculating equivalent volume, a spherical assumption is not always appropriate due to deformation, even if the particles were spherical when suspended. Particles may have a much larger projected-area diameter or "footprint" after impaction which would skew a volume calculation high, especially for particles with a significant coating of organic material.

Overall, aerosol particles are often analyzed after collection on a substrate where the role of the substrate is not clearly defined. Our understanding of atmospheric chemistry in the particle phase benefits from the precise measurement of these particles. Substrate effects influence particle size and behavior, particularly spreading along a surface. Well-characterized spreading can be used to assess some physical attributes of impacted aerosol particles (Olson et al. 2019; Morris et al. 2016; Lei et al. 2022; Ray et al. 2019), but disregarding the surface may lead to systematic bias in substrate-based measurements. The surprisingly high level of diversity in morphology and the deviation between suspended and impacted particle diameters found in this study implies that great care should be taken when comparing data sets from diverse instrumentation sources.

Associated Content

Supplemental Information can be found online and contains supporting experimental details including a flow tube schematic, TEM imaging protocols and further details on particle characterization, numerical data for additional SEM and AFM experiments and the assessment of organic material over time.

Acknowledgment

E.C.T., E.-J.E.O., and M.A.F. gratefully acknowledge support from NSF AGS-1916758. D.N.H., D.E.K., and M.V.J. gratefully acknowledge support from NSF AGS-1916819. The authors would like to thank J. N. Dawson for preliminary contributions to the project. We also

thank W. Auker and A. K. Hendrickson-Stives for assistance with particle and substrate characterizations respectively. We gratefully acknowledge D. D Dutcher for help with generation of secondary organic material at the Pennsylvania State University.

Funding

E.C.T., E.-J.E.O., and M.A.F. gratefully acknowledge support from NSF AGS-1916758.

D.N.H., D.E.K., and M.V.J. gratefully acknowledge support from NSF AGS-1916819.

References

- Alstadt, Valerie J., Kevin T. Jansen, Emily-Jean E. Ott, Muhammad Bilal Altaf, and Miriam Arak Freedman. 2018. "Local Aerosol Composition before and during the Transition from Coal-Fired Power to Natural Gas." *Atmospheric Environment* 190 (October): 169–76. https://doi.org/10.1016/j.atmosenv.2018.07.013.
- Altaf, Muhammad Bilal, Dabrina D. Dutcher, Timothy M. Raymond, and Miriam Arak Freedman. 2018. "Effect of Particle Morphology on Cloud Condensation Nuclei Activity." *ACS Earth and Space Chemistry* 2 (6): 634–39. https://doi.org/10.1021/acsearthspacechem.7b00146.
- Ault, Andrew P., and Jessica L. Axson. 2017. "Atmospheric Aerosol Chemistry: Spectroscopic and Microscopic Advances." *Analytical Chemistry* 89 (1): 430–52. https://doi.org/10.1021/acs.analchem.6b04670.
- Beaver, Melinda R., Rebecca M. Garland, Christa A. Hasenkopf, Tahllee Baynard, A. R. Ravishankara, and Margaret A. Tolbert. 2008. "A Laboratory Investigation of the Relative Humidity Dependence of Light Extinction by Organic Compounds from Lignin Combustion." *Environmental Research Letters* 3 (4): 045003. https://doi.org/10.1088/1748-9326/3/4/045003.
- Bell, Suzanne, and Keith Morris. 2010. An Introduction to Microscopy. Boca Raton: CRC Press.
- Bondy, Amy L., Rachel M. Kirpes, Rachel L. Merzel, Kerri A. Pratt, Mark M. Banaszak Holl, and Andrew P. Ault. 2017. "Atomic Force Microscopy-Infrared Spectroscopy of Individual Atmospheric Aerosol Particles: Subdiffraction Limit Vibrational Spectroscopy and Morphological Analysis." *Analytical Chemistry* 89 (17): 8594–98. https://doi.org/10.1021/acs.analchem.7b02381.
- Buseck, Peter R., Daniel J. Jacob, Mihály Pósfai, Jia Li, and J. R. Anderson. 2000. "Minerals in the Air: An Environmental Perspective." *International Geology Review* 42 (7): 577–93. https://doi.org/10.1080/00206810009465101.
- Charlson, R. J., S. E. Schwartz, J. M. Hales, R. D. Cess, J. A. Coakley, J. E. Hansen, and D. J. Hofmann. 1992. "Climate Forcing by Anthropogenic Aerosols." *Science* 255 (5043): 423–30. https://doi.org/10.1126/science.255.5043.423.
- Ching, Joseph, Kouji Adachi, Yuji Zaizen, Yasuhito Igarashi, and Mizuo Kajino. 2019. "Aerosol Mixing State Revealed by Transmission Electron Microscopy Pertaining to Cloud

- Formation and Human Airway Deposition." *Npj Climate and Atmospheric Science* 2 (1): 1–7. https://doi.org/10.1038/s41612-019-0081-9.
- Cohen, Liron, Maria Isabel Quant, and D. James Donaldson. 2020. "Real-Time Measurements of PH Changes in Single, Acoustically Levitated Droplets Due to Atmospheric Multiphase Chemistry." *ACS Earth and Space Chemistry* 4 (6): 854–61. https://doi.org/10.1021/acsearthspacechem.0c00041.
- Dahneke, Barton. 1971. "The Capture of Aerosol Particles by Surfaces." *Journal of Colloid and Interface Science* 37 (2): 342–53. https://doi.org/10.1016/0021-9797(71)90302-X.
- Dallemagne, Magda A., Xiau Ya Huang, and Nathan C. Eddingsaas. 2016. "Variation in PH of Model Secondary Organic Aerosol during Liquid–Liquid Phase Separation." *The Journal of Physical Chemistry A* 120 (18): 2868–76. https://doi.org/10.1021/acs.jpca.6b00275.
- Dang, Caroline, Michal Segal-Rozenhaimer, Haochi Che, Lu Zhang, Paola Formenti, Jonathan Taylor, Amie Dobracki, et al. 2022. "Biomass Burning and Marine Aerosol Processing over the Southeast Atlantic Ocean: A TEM Single-Particle Analysis." *Atmospheric Chemistry and Physics* 22 (14): 9389–9412. https://doi.org/10.5194/acp-22-9389-2022.
- DeCarlo, Peter F., Jay G. Slowik, Douglas R. Worsnop, Paul Davidovits, and Jose L. Jimenez. 2004. "Particle Morphology and Density Characterization by Combined Mobility and Aerodynamic Diameter Measurements. Part 1: Theory." *Aerosol Science and Technology* 38 (12): 1185–1205. https://doi.org/10.1080/027868290903907.
- Freedman, Miriam A., Kelly J. Baustian, Matthew E. Wise, and Margaret A. Tolbert. 2010. "Characterizing the Morphology of Organic Aerosols at Ambient Temperature and Pressure." *Analytical Chemistry* 82 (19): 7965–72. https://doi.org/10.1021/ac101437w.
- Freedman, Miriam Arak. 2017. "Phase Separation in Organic Aerosol." *Chemical Society Reviews* 46 (24): 7694–7705. https://doi.org/10.1039/C6CS00783J.
- Fu, H., Min Zhang, Wei Li, J. Chen, and Wei Wang. 2011. "Morphology, Composition and Mixing State of Individual Carbonaceous Aerosol in Urban Shanghai." *Atmospheric Chemistry and Physics Discussions* 11 (July): 20973–11. https://doi.org/10.5194/acpd-11-20973-2011.
- Gorkowski, Kyle, Neil M. Donahue, and Ryan C. Sullivan. 2020. "Aerosol Optical Tweezers Constrain the Morphology Evolution of Liquid-Liquid Phase-Separated Atmospheric Particles." *Chem* 6 (1): 204–20. https://doi.org/10.1016/j.chempr.2019.10.018.
- Higgins, Devon N., Michael S. Taylor, Justin M. Krasnomowitz, and Murray V. Johnston. 2022. "Growth Rate Dependence of Secondary Organic Aerosol on Seed Particle Size, Composition, and Phase." *ACS Earth and Space Chemistry* 6 (9): 2158–66. https://doi.org/10.1021/acsearthspacechem.2c00049.
- Kerecman, Devan E., Michael J. Apsokardu, Savannah L. Talledo, Michael S. Taylor, Devon N. Haugh, Yao Zhang, and Murray V. Johnston. 2021. "Online Characterization of Organic Aerosol by Condensational Growth into Aqueous Droplets Coupled with Droplet-Assisted Ionization." *Analytical Chemistry* 93 (5): 2793–2801. https://doi.org/10.1021/acs.analchem.0c03697.
- Krasnomowitz, Justin M., Michael J. Apsokardu, Christopher M. Stangl, Lee Tiszenkel, Qi Ouyang, Shanhu Lee, and Murray V. Johnston. 2019. "Growth of Aitken Mode Ammonium Sulfate Particles by α-Pinene Ozonolysis." *Aerosol Science and Technology* 53 (4): 406–18. https://doi.org/10.1080/02786826.2019.1568381.
- Lall, Anshuman Amit, and Sheldon K. Friedlander. 2006. "On-Line Measurement of Ultrafine Aggregate Surface Area and Volume Distributions by Electrical Mobility Analysis: I.

- Theoretical Analysis." *Journal of Aerosol Science* 37 (3): 260–71. https://doi.org/10.1016/j.jaerosci.2005.05.021.
- Laskin, Alexander, Mary K. Gilles, Daniel A. Knopf, Bingbing Wang, and Swarup China. 2016. "Progress in the Analysis of Complex Atmospheric Particles." *Annual Review of Analytical Chemistry* 9 (1): 117–43. https://doi.org/10.1146/annurev-anchem-071015-041521.
- Laskina, Olga, Holly S. Morris, Joshua R. Grandquist, Armando D. Estillore, Elizabeth A. Stone, Vicki H. Grassian, and Alexei V. Tivanski. 2015. "Substrate-Deposited Sea Spray Aerosol Particles: Influence of Analytical Method, Substrate, and Storage Conditions on Particle Size, Phase, and Morphology." *Environmental Science & Technology* 49 (22): 13447–53. https://doi.org/10.1021/acs.est.5b02732.
- Lee, Hansol D., Chathuri P. Kaluarachchi, Elias S. Hasenecz, Jonic Z. Zhu, Eduard Popa, Elizabeth A. Stone, and Alexei V. Tivanski. 2019. "Effect of Dry or Wet Substrate Deposition on the Organic Volume Fraction of Core–Shell Aerosol Particles." *Atmospheric Measurement Techniques* 12 (3): 2033–42. https://doi.org/10.5194/amt-12-2033-2019.
- Lei, Ziying, Nicole E. Olson, Yue Zhang, Yuzhi Chen, Andrew T. Lambe, Jing Zhang, Natalie J. White, et al. 2022. "Morphology and Viscosity Changes after Reactive Uptake of Isoprene Epoxydiols in Submicrometer Phase Separated Particles with Secondary Organic Aerosol Formed from Different Volatile Organic Compounds." *ACS Earth and Space Chemistry* 6 (4): 871–82. https://doi.org/10.1021/acsearthspacechem.1c00156.
- Li, Weijun, Xiaome Teng, Xiyao Chen, Lei Liu, Liang Xu, Jian Zhang, Yuanyuan Wang, Yue Zhang, and Zongbo Shi. 2021. "Organic Coating Reduces Hygroscopic Growth of Phase-Separated Aerosol Particles." *Environmental Science & Technology* 55 (24): 16339–46. https://doi.org/10.1021/acs.est.1c05901.
- McMurry, Peter H. 2000. "A Review of Atmospheric Aerosol Measurements." *Atmospheric Environment* 34 (12): 1959–99. https://doi.org/10.1016/S1352-2310(99)00455-0.
- Mikhailov, E., S. Vlasenko, S. T. Martin, T. Koop, and U. Pöschl. 2009. "Amorphous and Crystalline Aerosol Particles Interacting with Water Vapor: Conceptual Framework and Experimental Evidence for Restructuring, Phase Transitions and Kinetic Limitations." Atmospheric Chemistry and Physics 9 (24): 9491–9522. https://doi.org/10.5194/acp-9-9491-2009.
- Morris, Holly S., Armando D. Estillore, Olga Laskina, Vicki H. Grassian, and Alexei V. Tivanski. 2016. "Quantifying the Hygroscopic Growth of Individual Submicrometer Particles with Atomic Force Microscopy." *Analytical Chemistry* 88 (7): 3647–54. https://doi.org/10.1021/acs.analchem.5b04349.
- O'Brien, Rachel E., Alexander Neu, Scott A. Epstein, Amanda C. MacMillan, Bingbing Wang, Stephen T. Kelly, Sergey A. Nizkorodov, Alexander Laskin, Ryan C. Moffet, and Mary K. Gilles. 2014. "Physical Properties of Ambient and Laboratory-Generated Secondary Organic Aerosol." *Geophysical Research Letters* 41 (12): 4347–53. https://doi.org/10.1002/2014GL060219.
- Olson, Nicole E., Ziying Lei, Rebecca L. Craig, Yue Zhang, Yuzhi Chen, Andrew T. Lambe, Zhenfa Zhang, Avram Gold, Jason D. Surratt, and Andrew P. Ault. 2019. "Reactive Uptake of Isoprene Epoxydiols Increases the Viscosity of the Core of Phase-Separated Aerosol Particles." *ACS Earth and Space Chemistry* 3 (8): 1402–14. https://doi.org/10.1021/acsearthspacechem.9b00138.

- Ott, Emily-Jean E., and Miriam Arak Freedman. 2020. "Inhibition of Phase Separation in Aerosolized Water-Soluble Polymer–Polymer Nanoparticles at Small Sizes and the Effects of Molecular Weight." *The Journal of Physical Chemistry B* 124 (34): 7518–23. https://doi.org/10.1021/acs.jpcb.0c06535.
- Ott, Emily-Jean E., Theresa M. Kucinski, Joseph Nelson Dawson, and Miriam Arak Freedman. 2021. "Use of Transmission Electron Microscopy for Analysis of Aerosol Particles and Strategies for Imaging Fragile Particles." *Analytical Chemistry* 93 (33): 11347–56. https://doi.org/10.1021/acs.analchem.0c05225.
- Park, K., D. Dutcher, M. Emery, J. Pagels, H. Sakurai, J. Scheckman, S. Qian, et al. 2008. "Tandem Measurements of Aerosol Properties—A Review of Mobility Techniques with Extensions." *Aerosol Science and Technology* 42 (10): 801–16. https://doi.org/10.1080/02786820802339561.
- Park, Kihong, David B. Kittelson, and Peter H. McMurry. 2004. "Structural Properties of Diesel Exhaust Particles Measured by Transmission Electron Microscopy (TEM): Relationships to Particle Mass and Mobility." *Aerosol Science and Technology* 38 (9): 881–89. https://doi.org/10.1080/027868290505189.
- Pósfai, Mihály, and Peter R. Buseck. 2010. "Nature and Climate Effects of Individual Tropospheric Aerosol Particles." *Annual Review of Earth and Planetary Sciences* 38 (1): 17–43. https://doi.org/10.1146/annurev.earth.031208.100032.
- Prather, Kimberly A., Courtney D. Hatch, and Vicki H. Grassian. 2008. "Analysis of Atmospheric Aerosols." *Annual Review of Analytical Chemistry* 1 (1): 485–514. https://doi.org/10.1146/annurev.anchem.1.031207.113030.
- Radney, James G., Rian You, Xiaofei Ma, Joseph M. Conny, Michael R. Zachariah, Joseph T. Hodges, and Christopher D. Zangmeister. 2014. "Dependence of Soot Optical Properties on Particle Morphology: Measurements and Model Comparisons." *Environmental Science & Technology* 48 (6): 3169–76. https://doi.org/10.1021/es4041804.
- Ray, Kamal K., Hansol D. Lee, Miguel A. Gutierrez, Franklin J. Chang, and Alexei V. Tivanski. 2019. "Correlating 3D Morphology, Phase State, and Viscoelastic Properties of Individual Substrate-Deposited Particles." *Analytical Chemistry* 91 (12): 7621–30. https://doi.org/10.1021/acs.analchem.9b00333.
- Reid, Jonathan P., Allan K. Bertram, David O. Topping, Alexander Laskin, Scot T. Martin, Markus D. Petters, Francis D. Pope, and Grazia Rovelli. 2018. "The Viscosity of Atmospherically Relevant Organic Particles." *Nature Communications* 9 (1): 956. https://doi.org/10.1038/s41467-018-03027-z.
- Riemer, N., A. P. Ault, M. West, R. L. Craig, and J. H. Curtis. 2019. "Aerosol Mixing State: Measurements, Modeling, and Impacts." *Reviews of Geophysics* 57 (2): 187–249. https://doi.org/10.1029/2018RG000615.
- Rogak, Steven N., Richard C. Flagan, and Hung V. Nguyen. 1993. "The Mobility and Structure of Aerosol Agglomerates." *Aerosol Science and Technology* 18 (1): 25–47. https://doi.org/10.1080/02786829308959582.
- Seinfeld, John H., and Spyros N. Pandis. 2016. *Atmospheric Chemistry and Physics: From Air Pollution to Climate Change*. 3 edition. Hoboken, New Jersey: Wiley.
- Slade, Jonathan H., Andrew P. Ault, Alexander T. Bui, Jenna C. Ditto, Ziying Lei, Amy L. Bondy, Nicole E. Olson, et al. 2019. "Bouncier Particles at Night: Biogenic Secondary Organic Aerosol Chemistry and Sulfate Drive Diel Variations in the Aerosol Phase in a

- Mixed Forest." *Environmental Science & Technology* 53 (9): 4977–87. https://doi.org/10.1021/acs.est.8b07319.
- Sobanska, S., G. Falgayrac, J. Rimetz-Planchon, E. Perdrix, C. Brémard, and J. Barbillat. 2014. "Resolving the Internal Structure of Individual Atmospheric Aerosol Particle by the Combination of Atomic Force Microscopy, ESEM–EDX, Raman and ToF–SIMS Imaging." *Microchemical Journal* 114 (May): 89–98. https://doi.org/10.1016/j.microc.2013.12.007.
- Stolzenburg, Mark R., and Peter H. McMurry. 2008. "Equations Governing Single and Tandem DMA Configurations and a New Lognormal Approximation to the Transfer Function." *Aerosol Science and Technology* 42 (6): 421–32. https://doi.org/10.1080/02786820802157823.
- Tu, Peijun, and Murray V. Johnston. 2017. "Particle Size Dependence of Biogenic Secondary Organic Aerosol Molecular Composition." *Atmospheric Chemistry and Physics* 17 (12): 7593–7603. https://doi.org/10.5194/acp-17-7593-2017.
- Veghte, Daniel P., Muhammad Bilal Altaf, and Miriam Arak Freedman. 2013. "Size Dependence of the Structure of Organic Aerosol." *Journal of the American Chemical Society* 135 (43): 16046–49. https://doi.org/10.1021/ja408903g.
- Veghte, Daniel P., Muhammad Bilal Altaf, Joshua D. Haines, and Miriam Arak Freedman. 2016. "Optical Properties of Non-Absorbing Mineral Dust Components and Mixtures." *Aerosol Science and Technology* 50 (11): 1239–52. https://doi.org/10.1080/02786826.2016.1225153.
- Veghte, Daniel P., Danielle Rae Bittner, and Miriam Arak Freedman. 2014. "Cryo-Transmission Electron Microscopy Imaging of the Morphology of Submicrometer Aerosol Containing Organic Acids and Ammonium Sulfate." *Analytical Chemistry* 86 (5): 2436–42. https://doi.org/10.1021/ac403279f.
- Veghte, Daniel P., and Miriam A. Freedman. 2012. "The Necessity of Microscopy to Characterize the Optical Properties of Size-Selected, Nonspherical Aerosol Particles." *Analytical Chemistry* 84 (21): 9101–8. https://doi.org/10.1021/ac3017373.
- Wise, Matthew E., Scot T. Martin, Lynn M. Russell, and Peter R. Buseck. 2008. "Water Uptake by NaCl Particles Prior to Deliquescence and the Phase Rule." *Aerosol Science and Technology* 42 (4): 281–94. https://doi.org/10.1080/02786820802047115.
- You, Yuan, Lindsay Renbaum-Wolff, Marc Carreras-Sospedra, Sarah J. Hanna, Naruki Hiranuma, Saeid Kamal, Mackenzie L. Smith, et al. 2012. "Images Reveal That Atmospheric Particles Can Undergo Liquid–Liquid Phase Separations." *Proceedings of the National Academy of Sciences* 109 (33): 13188–93. https://doi.org/10.1073/pnas.1206414109.
- Zardini, A. A., S. Sjogren, C. Marcolli, U. K. Krieger, M. Gysel, E. Weingartner, U. Baltensperger, and T. Peter. 2008. "A Combined Particle Trap/HTDMA Hygroscopicity Study of Mixed Inorganic/Organic Aerosol Particles." *Atmospheric Chemistry and Physics* 8 (18): 5589–5601. https://doi.org/10.5194/acp-8-5589-2008.
- Zhang, Yue, Yuzhi Chen, Andrew T. Lambe, Nicole E. Olson, Ziying Lei, Rebecca L. Craig, Zhenfa Zhang, et al. 2018. "Effect of the Aerosol-Phase State on Secondary Organic Aerosol Formation from the Reactive Uptake of Isoprene-Derived Epoxydiols (IEPOX)." *Environmental Science & Technology Letters* 5 (3): 167–74. https://doi.org/10.1021/acs.estlett.8b00044.